Computing two dimensional flood wave propagation using unstructured finite volume method: Application to the Ourika valley

H. Belhadj[1]
[1] *Université Abdelmalek-Essaadi, Faculté des Sciences et Techniques, Dept. de Maths, Rte de Ziaten, B.P. 416 Tanger-Morocco*
hbelhadj@fstt.ac.ma

A. Taik[2]
[2] *Université Hassan II, Faculté des Sciences et Techniques, Dept. de Maths, UFR Mathématiques et Applications, Laboratoire MAC, B.P. 146, Mohammadia-Morocco*
taik_ahmed@yahoo.fr

D. Ouazar[3]
[3] *Université Mohammed V, Ecole Mohammadia d'Ingénieurs, Laboratoire LASH., Dept. Génie Civil., Avenue Ibn Sina -B.P. 765 -Agdal, Rabat-Morocco*
ouazar@emi.ac.ma

Abstract

This study is devoted to the flood wave propagation modelling corresponding to a realistic situation. The equations that governs the propagation of a flood wave, in natural rivers, corresponds to the free surface flow equations in the Shallow Water case. The obtained two dimensional system, known as Saint Venant's system, is derived from the three-dimensional incompressible Navier Stokes equations by depth-averaging of the state variables. This system is written in a conservative form with hyperbolic homogeneous part. The discretization of the convection part is carried out by the use of the finite volume method on unstructured mesh. To increase the accuracy of the scheme, the MUSCL technique is used. The diffusive part is discretized using a Green-Gauss interpolation technique based on a diamond shaped co-volume. For the numerical experiment, we have studied a realistic channel of the Ourika valley which is located in Morocco. The flood occurred on August 1995 is simulated with the objective of evaluating the behavior of the wave propagation in the channel. The results of the proposed numerical model gives velocities and free surface elevations at different stopped times of the simulation.

Key words : Shallow water equations, Finite volume method, Unstructured mesh, Roe scheme, Green-Gauss interpolation, Manning equation, Flood, Ourika valley

1 Introduction

Flooding is both a phenomenon which is either natural or involuntary caused by man-made changes in the environment, or even by a voluntary accidental human action. This flooding usually affects lands located close to a water course or water body with variable levels. It may regularly occur, in temperate and cold climatic zones for instance when snow melts, or in tropical and monsoon countries during the rainy season. It may be random or accidental when flooding is caused by exceptionally heavy rain or dam failure.

From the fluid mechanics point of view propagation is an extremely complicated phenomenon involving the dynamics of a fluid with a free boundary in intense turbulent motion under the acceleration of gravity. Recently, the problem of flood wave propagation, represent a great challenge in the mathematical modelling process. When trying to describe mathematically this situation, one is faced with solving a full three dimensional unsteady Navier-Stokes problem with a free boundary. It is well known, however that its not easy to compute if all the space and time scales involved during a flood are to be resolved.

If only the main features of the flow pattern are of interest and no attention is paid in resolving smaller scale effects such as secondary flows, boundary layers or turbulence, one may resort to a simpler mathematical representation of the physical reality. This is certainly the case in many engineering applications, where depending on the cause that produced the flood, its severity or the time interval to be modelled, a simple kinematic description can be sufficient to provide the requested answers.

In this work we shall be concerned with situation in which the full nonlinear Saint-Venant or Shallow Water equations are needed to account for dynamical effects such as propagation of water fronts. One feature of this set of hyperbolic equations is the formation of discontinuous solutions, which can be difficult to represent accurately. However, the development of finite volume methods for hyperbolic conservation laws has been a rapidly growing area for the last decade due to its attractive features and specifically nice shock capturing ([AG 94], [CHV 80], [TMO 05]).

The proposed mathematical model is discretized by using the finite volume method on unstructured mesh. The discretization uses a cell-centred finite volume formulation (see for example [BW 95]). The convective fluxe is approached using the Roe approximate Riemann solver (see [RPL 81], [LRJ 92]).

To increase the accuracy of the scheme, gradient information needs to be used. The states are supposed to be in a set of linear piecewise functions in each control volume. However, the obtained second order scheme is not monotone. To preserve the TVD (Total Variation Diminishing) property we have used the MUSCL (Monotonic Upstream Schemes for Conservations Laws) technique [YEE 89]. This procedure consists in limiting the gradient of the state variable on each element such that new extrema is not generated. To discretize the diffusive part, Green-Gauss type interpolation has been performed (see [CVV 96]). The gradient on each edge of a cell is approached using the Green theorem combined to an interpolation process developed to ensure the weak consistency of the scheme (see [CVV 96], [CVV 99]). Furthermore, an explicit Euler scheme for time integration is used.

For the numerical experiment, the proposed model is applied to the realistic situation of the Ourika valley that is located in the high Atlas mountain some forty kilometers south of the city of Marrakech in Morocco. The flood occurred on August $17, 1995$, is simulated in order to show the water depth profile at different stopped times of the simulation. In this intention one has the data of transverse profiles of the river given on 15 stations separated by $200m$ on average. The channel considered in this work is then $2800m$ long. The hydrograph of flow's rates measured at time of the flood at the station of Aghbalou (the upstream of the catchment area) is used as an upstream boundary condition. The other calculation parameters have been assessed on the basis of regional and bibliographical information. The results of this realistic application show the consistency of the suggested numerical model. This model could be used in the future as a basis for undertaking a study to build a system for managing the flood phenomenon with the objective of forecasting the flood events on the Ourika valley and on other areas.

The paper is organized as follows. In the next section, we define the governing equations. In section 3, we present formally the mathematical approach. In section 4, we carry out the numerical treatment of the convective part and the diffusive part, also convergence of the obtained scheme and numerical treatment of boundary conditions are discussed. The numerical experiment is fulfilled in section 5. In section 6, the flood simulation is presented. Finally in sections 7, 8, we discuss the obtained results and we end by some concluding remarks.

2 Governing equations

It is assumed that the flow is mainly two dimensional taking place in a horizontal plane $(x - y)$ parallel to the hearth surface, and being described by water depth H, and the two cartesian components of the the water velocity in the plane of motion, U, V. Any dependence of the flow variables on the vertical coordinate (z) is neglected and it is also assumed that the vertical velocity is zero. Considering a hydrostatic pressure distribution, the 2-D Saint-Venant equations can be derived by depth averaging the Navier-Stokes equations with appropriate boundary conditions (see [AM 05], [BH 06], [BOT 05] [TAI 02], [TMO 05]).

2.1 Shallow Water equations in two dimensions

The obtained $2 - D$ Shallow Water equations can be written as the following:

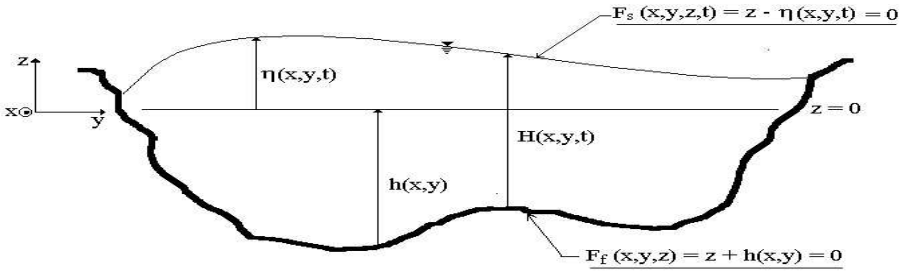

Figure 1: Description of the physical variables

$$
\begin{cases}
\dfrac{\partial H}{\partial t} + \dfrac{\partial (HU)}{\partial x} + \dfrac{\partial (HV)}{\partial y} = 0, \\
\dfrac{\partial (HU)}{\partial t} + \dfrac{\partial (UHU)}{\partial x} + gH\dfrac{\partial \eta}{\partial x} + \dfrac{\partial (VHU)}{\partial y} = \dfrac{1}{\rho}\dfrac{\partial}{\partial x}(\nu_t \dfrac{\partial (HU)}{\partial x}) \\
+\dfrac{1}{\rho}\dfrac{\partial}{\partial y}(\nu_t \dfrac{\partial (HU)}{\partial y}) + gH(S_{0x} - S_{fx}), \\
\dfrac{\partial (HV)}{\partial t} + \dfrac{\partial (UHV)}{\partial x} + gH\dfrac{\partial \eta}{\partial y} + \dfrac{\partial (VHV)}{\partial y} = \dfrac{1}{\rho}\dfrac{\partial}{\partial x}(\nu \dfrac{\partial (HV)}{\partial x}) \\
+\dfrac{1}{\rho}\dfrac{\partial}{\partial y}(\nu \dfrac{\partial (HV)}{\partial y}) + gH(S_{0y} - S_{fy}),
\end{cases} \tag{1}
$$

Where x, y are the horizontal coordinates, t is the time, $U = U(x, y, t)$ is the depth-averaged velocity in the x direction. $V = V(x, y, t)$ is the depth-averaged velocity in the y direction. $H = H(x, y, t)$ is the instantaneous water depth (see figure 1.). ν is the laminar viscosity, g stains for the gravity acceleration. S_{0x} and S_{0y} are the bottom bed slopes defined as: $S_{0x} = -\dfrac{\partial Z_f}{\partial x}$ and $S_{0y} = -\dfrac{\partial Z_f}{\partial y}$, Z_f being the bed elevation. S_{fx}, S_{fy} correspond to the bottom friction slopes, when approximated by the Manning formula take the form:

$$
S_{fx} = \frac{n^2 U\sqrt{U^2+V^2}}{H^{\frac{4}{3}}} \qquad , \qquad S_{fy} = \frac{n^2 V\sqrt{U^2+V^2}}{H^{\frac{4}{3}}} \tag{2}
$$

where n is the Manning roughness coefficient.

Written in general conservative form the Saint-Venant equations in two dimensions read:

$$
\frac{\partial W}{\partial t} + \frac{\partial F(W)}{\partial x} + \frac{\partial G(W)}{\partial y} = R_x(W) + R_y(W) + S(W) \tag{3}
$$

Here : W is the vector of flow variables, F and G are the cartesian components of momentum flux.

$$
W = (H, q_u = HU, q_v = HV)^T,
$$

$$F(W) = (q_u, \frac{q_u^2}{H} + \frac{gH^2}{2}, \frac{q_u q_v}{H})^T, G(W) = (q_v, \frac{q_u q_v}{H}, \frac{q_v^2}{H} + \frac{gH^2}{2})^T,$$

$$R_x(W) = (0, \frac{\partial}{\partial x}(\nu\frac{\partial q_u}{\partial x}), \frac{\partial}{\partial x}(\nu\frac{\partial q_v}{\partial x}))^T, R_y(W) = (0, \frac{\partial}{\partial y}(\nu\frac{\partial q_u}{\partial y}), \frac{\partial}{\partial y}(\nu\frac{\partial q_v}{\partial y}))^T,$$

$$S(W) = (0, S_u, S_v)^T, S_u = gH(S_{0x} - S_{fx}), S_v = gH(S_{0y} - S_{fy})$$

$R_x(W)$ and $R_y(W)$ are a diffusive terms, $S(W)$ is a source term.

We note that source term of (3) is stiff , implementing it directly causes a numerical instability as it was shown by Ambrosi [AD 95] for a simple explicit discretization of source term integrated in the finite volume scheme for 1D Shallow Water model.

An alternative approach is to employ a time-splitting in which one alternative between solving a system of conservation laws, with no source terms, and a system of ordinary differential equations modelling the source terms ([LRJ 90], [CBMOB 96], [BME 98], [MLA 97]). In the simplest case this splitting takes the form [YEE 89]:

$$W^{n+1} = L_s^h L_f^h W^n \ ,$$

where L_f^h represent the numerical solution operator for the conservation law:

$$\frac{\partial W}{\partial t} + \frac{\partial F(W)}{\partial x} + \frac{\partial G(W)}{\partial y} - R_x\left(W\right) - R_y\left(W\right) = 0.$$

over the time $h = \Delta t$, and L_s^h the numerical solution operator for the ODE:

$$\frac{\partial W}{\partial t} = S(W) \ .$$

In this work, for simplicity, the bottom bed slopes and the roughness coefficient n are sated equal to zero, the source term is then neglected.

2.2 Boundary conditions

The above set of equations should be supplemented by a set of initial and appropriate boundary conditions to obtain a well posed problem.

Both of the water depth and the depth-averaged x and y velocity components need to be specified as initial condition:

$$W(x, y, 0) = W_0(x, y).$$

The same water surface elevation is assigned to every node point in a finite volume network and velocity is zero everywhere. Physically, there are two types of boundaries: Solid boundary and open boundary. The flow across a solid boundary generally equals to zero. In addition, either the tangential velocity or tangential stress needs to be specified on a solid boundary. On the open boundary the value are usually unknown and experience is needed to specify physically realistic values for engineering application. In our case we take Neumann condition.

3 Mathematical approach

One can formally write the problem under the following form :

Find $W \in C^0([0,t], H(\Omega))$ such that :

$$\begin{cases} \dfrac{\partial W}{\partial t} + \dfrac{\partial F(W)}{\partial x} + \dfrac{\partial G(W)}{\partial y} = R_x(W) + R_y(W) + S(W) \quad in\ \Omega, \\ \alpha W + \beta \dfrac{\partial W}{\partial x} = g \qquad\qquad over\ \Gamma = \partial\Omega, \\ W(x,0) = W_0(x) \qquad\qquad in\ \Omega. \end{cases} \tag{4}$$

Where: $W \in C^0([0,T],\ H(\Omega))$, Ω is a bounded open set of R^2, $\Gamma = \partial\Omega$, and $H(\Omega)$ is an Hilbert space, which is $L^2(\Omega)$ herein .

For such a complicated set of equations, it is rather difficult to derive a solution of (4) in the strong meaning or even to prove the existence and uniqueness of this solution. Nevertheless, physicists assure us that under realistic assumptions, physical solutions do exist.

We seek here to compute a weak solution of the problem by first writing an approximation of the temporal derivation which gives :

For $W^n \in L^2(\Omega)$, find $W^{n+1} \in L^2(\Omega)$ such that :

$$W^{n+1} = W^n + \Delta t\ A(W^n).$$

Where A is an operator including the transport terms, the diffusive terms and the source terms of the PDE. More specifically

$$A(W) = -\frac{\partial F}{\partial x}(W) - \frac{\partial G}{\partial y}(W) + R_x(W) + R_y(W) + S(W).$$

Since we are not sure that those terms are differentiable in the classical sense, we consider the last equation in the sense of the theory of distributions which is equivalent to writing :

$$\langle W^{n+1}, \Phi\rangle_{L^2(\Omega)} = \langle W^n + \Delta t\ A(W^n), \Phi\rangle_{L^2(\Omega)} \qquad \forall \Phi \in D'(\Omega), \tag{5}$$

To obtain an approximation of W^{n+1}, we make a projection of (5) in a finite dimension subspace V_h of $\mathrm{L}^2(\Omega)$. Thus we rewrite our problem:

For $W^n \in V_h(\Omega)$, find $W^{n+1} \in V_h(\Omega)$ such that :

$$\langle W^{n+1}, \Phi_i\rangle_{L^2(\Omega)} = \langle W^n + \Delta t\ A(W^n), \Phi_i\rangle_{L^2(\Omega)}, \qquad \forall \Phi \tag{6}$$

Where $(\Phi_i)_{i=1,\dots M}$ is a basis of $V_h(\Omega)$. More precisely, we consider a partition of Ω in finite volume cells $C_{i=1,\dots,nc}$ and take the basis of $V_h(\Omega), (\chi_i)_{i=1,\dots,nc}$, where χ_i is the characteristic function of the cell C_i .

Equation (5) can now be written as :

$$\langle W^{n+1}, \chi_i\rangle_{L^2(\Omega)} = \langle W^n + \Delta t\ A(W^n), \chi_i\rangle_{L^2(\Omega)}. \tag{7}$$

4 Spatial discretization

The advantage of the unstructured meshes is that they can be applied to the complex geometries. In this type of mesh, at each node, the connection with the neighbors ones must be explicitly defined in the connectivity matrix.

In this work, the unstructured mesh is composed of triangles, (see figure 6) show meshes generated by using the Dalaunay triangulation technique. We use the "Cell-Centred" formulation which all the state variables are updated at the centroid of each cell. Integration of the system (3) over a control volume C_i and Gauss divergence formulas lead to:

$$meas(C_i)\frac{\partial W_i}{\partial t}+\int_{\partial C_i}(F(W)n_x+G(W)n_y)d\sigma=\int_{C_i}(R_x(W)+R_y(W))d\sigma+\int_{C_i}S(W)d\sigma$$

(n_x, n_y) are the components of the outward unit normal to ∂C_i.

4.1 Numerical treatment of the convection

There are several ways to carry out the convection flux (here we present an upwind scheme based on a Roe's approximate Riemann solver). Consider the hyperbolic part of equation (3) given by:

$$\frac{\partial W}{\partial t}+\frac{\partial F(W)}{\partial x}+\frac{\partial G(W)}{\partial y}=0 \tag{8}$$

Integrating the equation (8) on a control volume C_i and using assumption that W is constant by volume, it comes:

$$meas(C_i)\frac{\partial W_i}{\partial t}+\int_{\partial C_i}(F(W)n_x+G(W)n_y)d\sigma=0 \tag{9}$$

Here W_i is the value of W on cell C_i.

Let

$$IF(W)=F(W)n_x+G(W)n_y$$

The integral term can be written as

$$\int_{\partial C_i}IF(W)d\sigma=\sum_j\int_{\Gamma_{ij}}IF(W)d\sigma \tag{10}$$

Γ_{ij} is the interface between the cells C_i , C_j for all triangle C_j having a common edge with the cell C_i.

To evaluate the integral over the interface Γ_{ij}, we use the following approximation

$$\int_{\Gamma_{ij}}IF(W)d\sigma=\Phi(W_i,W_j,n_{ij})meas(\Gamma_{ij}) \tag{11}$$

Roe proposed a particular choice of $\Phi(W_i, W_j, n_{ij})$ based on the resolution at each time step of approximate linear Riemann problems on each cell boundary of the mesh, knowing the initial left state W_i and the right state W_j (see [LRJ 90], [LRJ 92], [RPJ 81]):

$$\begin{aligned}\Phi(W_i, W_j, \vec{n}_{ij}) = &\frac{1}{2}(IF(W_i, \vec{n_{ij}}) + IF(W_j, \vec{n_{ij}})) \\ &-\frac{1}{2}\left|B(\widetilde{W}, \vec{n}_{ij})\right|(W_j - W_i),\end{aligned} \tag{12}$$

where $B(\widetilde{W}, \vec{n}_{ij})$ is an average Jacobian matrix, W_i and W_j are the initial left state and right state of the interface Γ_{ij}. The Roe-averaged value $\tilde{W}$ is related to W_i and W_j and is taken such that the conservativity condition is satisfied exactly

$$IF(W_j) - IF(W_i) = B(\tilde{W}, \vec{n}_{ij})(W_j - W_i).$$

On other side, the temporal term is discretized using an explicit Euler scheme lake:

$$\frac{\partial W_i}{\partial t} = \frac{W_i^{n+1} - W_i^n}{\Delta t}.$$

The finite volume scheme is then expressed by

$$W_i^{n+1} = W_i^n + \frac{\Delta t}{meas(C_i)} \sum_j meas(\Gamma_{ij})\Phi(W_i, W_j). \tag{13}$$

4.2 MUSCL thechnique

The scheme described above is a first order accurate scheme. This scheme is monotone but has a poor accuracy due to the large amount of numerical dissipation. For a higher order interpolation, gradient information needs to be used. The states are supposed now to be in a set of linear piecewise functions in each control volume. At the interface Γ_{ij}, left and right states W_{ij}^- and W_{ij}^+ are defined by [EBV 99]:

$$\begin{cases} W_{ij}^- = W_i + \dfrac{1}{2}\nabla W_i.\overrightarrow{G_iG_j}, \\ \\ W_{ij}^+ = W_j - \dfrac{1}{2}\nabla W_j.\overrightarrow{G_iG_j} \end{cases} \tag{14}$$

where G_i and G_j are respectively the barycenters of cells C_i, C_j. ∇W_i represents the gradient at the cell C_i. This term can be evaluated by minimizing the quadratic functional (see [CVV 96], [EBV 99])

$$\Psi_i(x, y) = \sum_{j \in K(i)} \left|W_i + (x_j - x_i)X + (y_j - y_i)Y - W_j\right|^2,$$

where $K(i)$ is the indices set of neighborhood triangles that have common edge or vertex with the triangle C_i, (x_i, y_i) are the barycenter coordinates of cell C_i. However, the obtained second order scheme is not monotone. To preserve the TVD property [YEE 89], we use the MUSCL technique [YEE 89]. This procedure consists in limiting the gradient of W on each element such that new extrema is not generated. The limited gradients is calculated as follows:

$$\frac{\partial^{\lim} W_i}{\partial x} = \frac{1}{2}[\min_{j \in K(i)} sgn(\frac{\partial W_j}{\partial x}) + \max_{j \in K(i)} sgn(\frac{\partial W_j}{\partial x})] \min_{j \in K(i)} \left|\frac{\partial W_j}{\partial x}\right|.$$

$\frac{\partial^{\lim} W_i}{\partial y}$ is evaluated in the same way. Then, interpolated left and right values are obtained by replacing in (12) the gradients ∇W_i and ∇W_j respectively with $\nabla^{\lim} W_i$ and $\nabla^{\lim} W_j$. Afterward , Roe numerical flux is calculated by writing:

$$\int_{\Gamma_{ij}} IF(W)d\sigma = \Phi(W_i^-, W_j^+, \overrightarrow{n_{ij}})meas(\Gamma_{ij})$$

The second order finite volume scheme using MUSCL technique is then expressed as follows

$$W_i^{n+1} = W_i^n + \frac{\Delta t}{meas(C_i)} \sum_j meas(\Gamma_{ij})\Phi(W_i^-, W_j^+). \tag{15}$$

4.3 The diffusive flux

When discretizing the diffusive terms , on has to evaluate $\int_{C_i} R_x(W)dv$ and $\int_{C_i} R_y(W)dv$ where $R_x(W) = \frac{\partial}{\partial x}\Big(\nu \frac{\partial q_u}{\partial x}\Big)$, and $R_y(W) = \frac{\partial}{\partial y}\Big(\nu \frac{\partial q_v}{\partial y}\Big)$, using Gauss divergence formula, we can write (for example):

$$\int_{C_i} \frac{\partial}{\partial x}(\nu \frac{\partial q_u}{\partial x})dv = \int_{\partial C_i} \nu \frac{\partial q_u}{\partial x} d\sigma = \sum_j \int_{\Gamma_{ij}} \nu \frac{\partial q_u}{\partial x} d\sigma,$$

then one has to evaluate terms such as:

$$\int_{\Gamma_{ij}} a' \frac{\partial a}{\partial x} n_x \, d\sigma \qquad \text{and} \qquad \int_{\Gamma_{ij}} b' \frac{\partial b}{\partial y} \, n_y \, d\sigma$$

where a (respectively b) is either q_u or q_v, a' (respectively b') is ν.

We use a Green-Gauss type interpolation to construct the gradients at the interface of the mesh. The gradient on each edge is approached by the Green theorem and then a first order Gauss quadrature formula, to obtain requisite values at the vertices P. The weak consistency of this scheme is proved under some assumption on the weights of interpolation (see [CVV 99]).

We have exploited this idea to handle our much more difficult problem, and discretize the diffusive part. We begin by writing

$$\int_{\Gamma_{ij}} \left(a' \frac{\partial a}{\partial x} \right) n_x \, d\sigma \; = \; a'_{|\Gamma_{ij}} \, \frac{\partial a}{\partial x}|_{\Gamma_{ij}} \int_{\Gamma_{ij}} n_x \, d\sigma. \tag{16}$$

The remaining problem is to evaluate a' and $\frac{\partial a}{\partial x}$ at the interface Γ_{ij} between two cells C_i and C_j.

One constructs the co-volume C_{dec} (called diamond shaped co-volume) centered at the interface Γ_{ij} and connecting the barycenters G_i and G_j of the triangles that share this edge and the two end points N and S (see figure 2).

To discretize $\frac{\partial a}{\partial x}|_{\Gamma_{ij}}$, the divergence theorem is applied to the co-volume C_{dec}, surrounding Γ_{ij}, which gives the approximation:

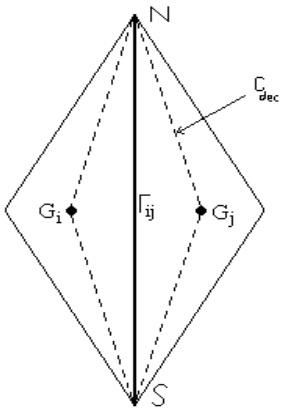

Figure 2: Diamond shaped co-volume

$$\frac{\partial a}{\partial x}|_{\Gamma_{ij}} \simeq \frac{1}{meas(C_{dec})} \sum_{\varepsilon \in \partial C_{dec}} a_{|_\varepsilon} \int_\varepsilon n_{x\varepsilon}\, d\sigma \qquad , \tag{17}$$

ε represents one edge of co-volume C_{dec} and $n_{x\varepsilon}$ is the axial component of the outward unit normal to ε.

If we note $\varepsilon = [N_1, N_2]$, one can also write:

$$\frac{\partial a}{\partial x}|_{\Gamma_{ij}} \simeq \frac{1}{meas(C_{dec})} \sum_{\varepsilon \in \partial C_{dec}} \frac{1}{2}(a_{N_1} + a_{N_2}) \int_\varepsilon n_{x\varepsilon}\, d\sigma \tag{18}$$

Where a_{N_1} and a_{N_2} are respectively the values of the state a on the node N_1 and N_2 of the edge ε.

The data at the centers G_i and G_j are known exactly while the data at the vertices N and S must be determined by some interpolation procedure. For one node P of the mesh, one utilizes a linear approximation v of a on the set of cells which share the vertex P . One writes

$$a_P = \sum_{K \in V(P)} \alpha_K(P) a_K.$$

Where $V(P)$ is the set of triangles K surrounding P, a_K the state at the center of triangle K and $\alpha_K(P)$ are the weights of the interpolation.

To ensure the weak consistency of the scheme described above, the weights $\alpha_K(P)$ are calculated by a least square approximation method (see [CVV 96], [EBV 99]). The idea is to minimize the quadratic function

$$L_P(v) = \sum_{K \in V(P)} (a_K - v(G_K))^2,$$

where v is a linear approximation of a on set of cells that share the vertex P,

$$v(x,y) = \beta_1 + \beta_2(x - x_P) + \beta_3(y - y_P),$$

that gives after some simple calculations and remarking that $v(x_P, y_P) = a_P = \beta_1$,

$$\alpha_K(P) = \frac{1 + \lambda_x(x_K - x_P) + \lambda_y(y_K - y_P)}{n_P + \lambda_x R_x + \lambda_y R_y}.$$

Where:

$$n_P = card(V(P)),\ \ R_x = \sum_{K \in V(P)} (x_K - x_P)\ ,\ R_y = \sum_{K \in V(P)} (y_K - y_P),$$

$$\lambda_x = \frac{I_{xy}R_y - I_{yy}R_x}{D}\ ,\ \lambda_y = \frac{I_{xy}R_x - I_{xx}R_y}{D},$$

$$I_{xx} = \sum_{K \in V(P)} (x_K - x_P)^2 \ \ I_{yy} = \sum_{K \in V(P)} (y_K - y_P)^2, I_{xy} = \sum_{K \in V(P)} (x_K - x_P)(y_K - y_P)$$

and

$$D = I_{xx}I_{yy} - I_{xy}^2.$$

Let's denote by $\Phi_{nv}(W)$ the flux coming from the convective part and $\Phi_v(W)$ the flux coming from the diffusive part. Since the source term is neglected, the global scheme can be written as:

$$W_{ij}^{n+1} \ = \ W_{ij}^n - \frac{\Delta t}{meas(C_i)}\Phi_{nv}(W_{ij}^n) + \frac{\Delta t}{meas(C_i)}\Phi_v(W_{ij}^n) \tag{19}$$

4.4 Convergence of the scheme

In [CVV 99], the authors showed the convergence of finite volume methods for the problem of the diffusion-convection on completely unstructured meshes, assuming the hypotheses of weak consistency and coercivity. In the case of the diamond-path scheme, what corresponds to our case, it has been proven a general result of consistency and a specific result of coercivity and so of convergence on regular meshes of quadrangles, resulting from the initial triangular unstructured mesh, by using diamond shaped co-volume technique (figure 2).

Typically, our calculations are begun with initial conditions corresponding to uniform flow at the reference state. This can cause severe start-up problems for flows around realistic geometries, where a large transient in the residuals can cause negative elevation H, which can sometimes kill the calculation. To overcome this problem, a CFL cutback procedure is used, which limits the maximum relative change in H per time step [CWJ 94]. In our case the following CFL condition relating to the convective part is used

$$CFL = \Delta t. \max(q_i \left|\lambda_{ij_k}\right| / meas(C_i)) \leq 1,$$

where q_i is the number of triangles surrounding the vertex a_i, λ_{ij_k} is the k^{th} eigenvalue of $A = \dfrac{\partial F(W)}{\partial x}n_x + \dfrac{\partial G(W)}{\partial y}n_y$.

4.5 Boundary conditions

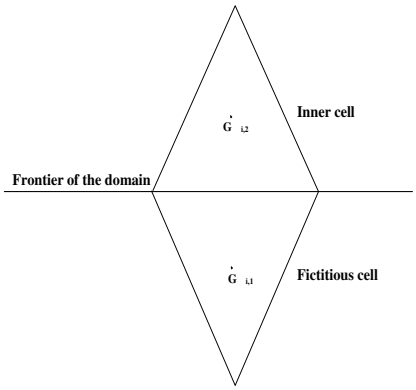

Figure 3: fictitious cells

The physical domain is surrounded by fictitious cells (figure 3). These cells are constructed by taking the symmetry of the inner ones of the domain. The frontier of the domain coincides with the frontiers which separate the fictitious cells and the inner cells. So the south border of the domain is composed of the north frontiers of the fictitious cells of the first line of the mesh. We consider the Dirichlet and Neumann boundary conditions which are approximated by the following

$$W_{i,boundary} \simeq \frac{1}{2}\left(W_{i,1} + W_{i,2}\right), \tag{20}$$

$$\left(\frac{\partial W}{\partial n}\right)_{i,boundary} \simeq \frac{1}{dist(G_{i,1}, G_{i,2})}\left(W_{i,1} - W_{i,2}\right), \tag{21}$$

$W_{i,1}$ is the value of W on the fictitious cell $(i,1)$, $G_{i,.}$ is the barycenter of cell $(i,.)$, $\dfrac{\partial}{\partial n}$ is the outer normal derivative.

Through this simple formula we can find what we must impose as the value of W on the fictitious cells depending on the boundary condition considered.

5 Numerical experiment: Ourika valley flood

Let us note that the characteristics data, which are provided below on the Ourika channel, was extracted from a bibliographical information.

5.1 Geometrical data of Ourika Channel

The characteristics channel form (Surface, perimeter, mirror width, and slope of the channel.) are determined from the data of transverse profiles of the river given on 15

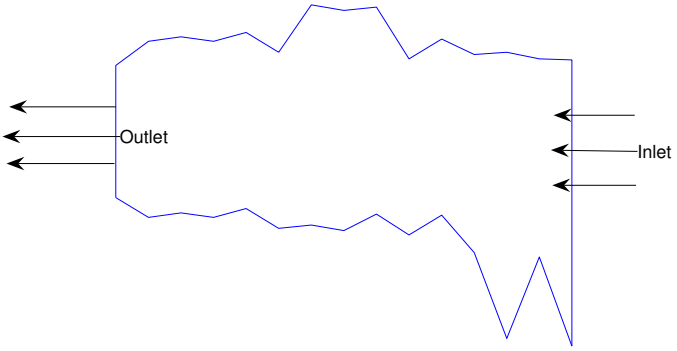

Figure 4: Geometry of the Ourika channel $200m \leq x \leq 3000m$ and $-925m \leq y \leq 625m$

stations. These stations are separated on average by $200m$. The channel considered here is then $2800m$ long. The geometry of the channel is provided in Figure 4.

5.2 Physical data of Ourika Channel

The physical data of the Ourika channel is provided by the measured flows during the flood event. The hydrograph of flow measured at the time of the flood in the station of Aghbalou is used as an upstream boundary condition. The instantaneous measured flows are given in table 1 provided below and represented in figure 5.

17/08/95	Times	Measured Flows (m3/s)
	8 h	0,55
	12 h	0,513
	16 h	0,513
	20 h	129,3
	20 h 30	1030
	21 h	70,45
	22 h	35,33
	23 h	34,27
18/08/95	8 h	10,31
	9 h	10
	10 h	9,4
	11 h	8,82
	12 h	8,26
	13 h	7,98
	14 h	7,72
	16 h	7,2
	18 h	6,7
	20 h	6,45
	22 h	6,22

Table 1: Measured flows at the inlet station (Aghbalou)

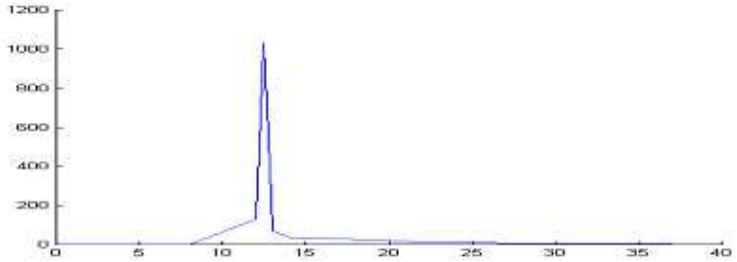

Figure 5: Flow hydrograph versus time

5.3 Boundary conditions at the inlet of the channel

At the upstream station, the channel has a strong slope ($S_0 = 0.05$), the flow is then considered supercritical. It becomes consequently necessary to apply in addition to

the hydrograph $Q(t)$ a second condition concerning the water elevation $H(t)$ at its inlet section. The method suggested in [FDL 88] allows to generate the hydrograph of water elevations $H(t)$ starting from $Q(t)$ and of the Manning equation applied to the inlet section. This technique was used in the one-dimensional hydrodynamic flood model DAMBRK (see [FRH 85], [FDL 77] and [FDL 82]). For a given flow discharge $Q(t)$, the Manning equation is the implicit nonlinear equation for $H(t)$ expressed as follows:

$$Q = (\phi/n)A_s R^{3/2} S^{1/2} \tag{22}$$

Where $\phi = 1$ in S.I units, R is the hydraulic radius, S the channel slope at the section, A_s the cross sectional area of flow and n the roughness coefficient. The hydraulic radius is provided by $R = A_s/P$ where P is the wetted perimeter. The approximate trapezoidal form of the upstream section, in the Ourika case, allows then to express A_s and P according to $H(t)$ [BH 06]. The solution of equation (2) using an iterative method (Newton method for example), gives the hydrograph of $H(t)$ and then the mean velocities by the relation $V = Q/A_s$. The obtained results are gathered in table 2.

TIME (t)	FLOWS Q(t) (m3/s)	ELEVATIONS H(t) (m)	MEAN VELOCITIES V(t) (m/s)
17 /08/1995			
8H	0.55	0.0149	0.2978
10H	0.513	0.0143	0.2895
16H	0.513	0.0143	0.2895
20H	129.3	0.3772	2.3303
20H30	1030	1.1714	4.4495
21H	70.45	0.2660	1.8919
22H	35.33	0.1779	1.4780
23H	34.27	0.1714	1.4927
18 /08/ 1995			
8H	10.31	0.0860	0.9330
9H	10	0.0844	0.9228
10H	9.4	0.0814	0.9008
11H	8.82	0.0783	0.8800
12H	8.26	0.0753	0.8583
13H	7.98	0.0738	0.8467
14H	7.72	0.0724	0.8355
16H	7.2	0.0694	0.8141
18H	6.7	0.0665	0.7918
20H	6.45	0.0650	0.7804
22H	6.22	0.0636	0.7697

Table 2: Mean velocities on upstream section (m/s)

6 Flood simulation

To simulate the wave propagation in the computational domain of figure 6 using the proposed numerical model, the following data concerning the geometry of the channel, initial and boundary conditions are taken into account.

- Unstructured mesh triangulation is of cell-centered type.
- Number of elements/nodes: 1102/609 (see figure 6).
- Length of the channel = $2800m$.
- Initial time step : $\Delta t = 0.01s$.
- CFL value = 0.7.
- $H = 10m$ anywhere in the channel at $t = 0$.
- $U = -0.29m/s$ and $V = 0m/s$ at $t = 0$ (in agreement with the hydrograph of velocities).
- At the inlet: mean velocities are given in table 2 as a boundary condition.
- At the solid boundaries: normal velocities are taken equal to zero.
- At the outlet: the Newmann condition. $\partial_n U = \partial_n V = 0$ is considered.

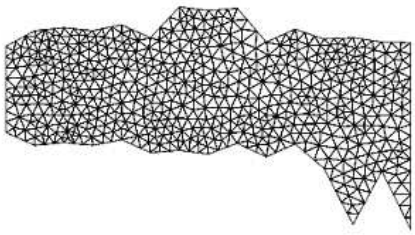

Figure 6: $2D$ grid of Ourika channel: $1102E/609N$

7 Results and discussion

At the time $20h30$, the velocity on the upstream section gone up $4.45m/s$ (see Table 2). To cross the considered channel of the valley ($2800m$) the flooding wave need approximately $10.5mn$.

Figures $7, 8, 9, 10, 11, 12$ illustrates respectively the evolution of the water wave propagation (iso-values of the velocity) in the channel at the following chosen stopped

times of the simulation: $t_1 = 20h31$, $t_2 = 20h32$,$t_3 = 20h34$, $t_4 = 20h36$, $t_5 = 20h38$ and $t_6 = 22h$.

Figures $7a, b; 8a, b; 9a, b; 10a, b; 11a, b; 12a, b$ show respectively results of the water depth profile for the same above stopped times of the simulation, the index a and b correspond respectively to the position $y = -239m$, $y = 127m$. The water elevation in the channel reaches approximately between 0 and 2 meters in comparison with the initial surface level.

Figures $13a, b, c, d, e, f$ show the evolution of the water depth (free surface in $3D$) for the same above stopped times of the simulation. We remark clearly the evolution of the flooding wave. The amplitude of the elevation is important around the times where the flood is occurred, for $t = 22h$, passing the period of the flood the amplitude of the elevation decrease and becomes normal.

Finally, figure 14 illustrate the evolution of depth versus time in seconde for 4 points in x-direction of the channel along the y-direction. It confirm the remark cited above.

8 Conclusion

In this work, we developed a robust solver for the $2D$ Saint Venant equations based on Roe's approximate Riemann solver with MUSCL technique for the convective part and Green-Gauss type interpolation for the viscous part (unstructured mesh case).

Also we presented our contribution to the modelling of the flood of Ourika valley (Morocco) produced the summer of 1995 . The obtained results show the consistency of the mathematical and numerical model. A comparison between the results of this model with the experimental results was wished in this work to gauge (calibration) the model. Unfortunately one does not have data for this fact.

A natural continuity of this work is to take a complete model, holding account particularly source term, if required to take a model of cloture to hold in account the effect of turbulence and pollutant transport model that would permit simulation of many environmental problems occurring.

9 Bibliography

[AG 94] Alcrudo F., Navarro P. G., (1994) "Computing two dimensional flood propagation with high resolution extension of Mccormack's method", Proceeding of the specialty conference, "Modelling of flood propagation Over Initially Dry Areas", 29 June-1 July, pp 3-17

[AM 05] Alcrudo F., Mulet J., (July 2005), "Urban inundation models based on the Shallow Water equations. Numerical and practical issues", FVCA4, Hermes Science Publishing, ISBN 1 905209 48 7, pp. 3-12

[AD 95] Ambrosi D., (1995), "Approximation of Shallow Water equations by Riemann solvers". Inter. Journ. for Numerical Methods in Fluids, 20, 157-168.

[BH 06] Belhadj H., (2006), "Résolution du système couplé Saint Venant / Transport utilisant la méthode des volumes finis et une technique de décomposition de domaine: Applications la modélisation des phénomènes de crue et de rupture de barrage" , thèse d'état, EMI (LASH), Agdal, Rabat, Maroc. A soutenir.

[BOT 05] Belhadj H., Ouazar D., Taik A. , (July 2005), "Unstructured finite volume for modelling the flood wave propagation: Application to the Ourika valley", FVCA4, Hermes Science Publishing, ISBN 1 905209 48 7, pp 551-560

[BME 98] Benkhaldoun F., Monthe L., Elmahi I., (1998), "A splitting finite volume Roe scheme for Shallow Water equations with source terms", Proc. CADAM Wallingford meeting, March, 2-3, Wallingford, UK.

[BW 95] Berzins M., Ware J.M., (1995), "Positive cell-centred finite volume discretisation methods for hyperbolic equations on irregular meshes", Appl. Numer. Math., Vol. 16, pp. 417-438.

[CBMOB 96] Chakir M., Benkhaldoun F., Monthe L., Ouazar D., Belghit A., (1996), "A Nine Point Finite Volume Roe Scheme for Shallow Water Equations Coupled to Pollutant Transport Including Source Terms", First International Symposium on Finite Volumes for Complex Applications, Rouen, July 15-18, Pbs. Hermes, pp 625-633.

[CWJ 94] Coirier W.J., (1994), "An Adaptively Refined , Cartesian, CellBased Scheme for the Euler and Navier-Stokes Equations". PhD thesis, University of Michigan.

[CHV 80] Cunge J.A., Holley F.M., Verwey A., (1980)," Practical Aspects of Computational River Hydraulics Monographs and Surveys in Water Resources Engineering", Pitman, Boston.

[CVV 96] Coudiere Y., Vila J.P. and Villedieu P. , (1996), " Convergence of a finite volume scheme for a diffusion problem", In F. Benkhaldoun, and R. Vilsmeier eds, FVCA, (Hermes, Paris), pp. 161-168.

[CVV 99] Coudiere Y., Vila J.P. and Villedieu P., (1999), "Convergence rate of a finite volume scheme for two dimensional convection-diffusion problem", Math. Model. Numer. Anal., vol. 33, pp 493-516.

[EBV 99] Elmahi I., Benkhaldoun F., Vilsmeier R., Gloth O., Patschull A. and Hanel, (1999), "Finite volume simulationof a droplet flame ignition on unstructured meshes", J. of Comput. and Appl. Math., Vol 103, 1, pp. 187-205.

[FDL 77] Fread D.L, (1977), "The development and testing of dam break flood forecasting model. Actes de l'atelier: "Dam-Break Flood Model" , Bethesda, MD , US

Water Ressources Council, Task Force on Dam Break Flood rooting, pp. 164-197.

[FDL 82] Fread D.L, (1982), "DAMBRK: The NWS Dam-Break Flood Forecasting Model", National Weather Service, Office of Hydrology, Silver Spring, Md, Jan.

[FDL 88] Fread D.L, (1988), "The NWS Dam-Break Model: Theoretical Background" / User Documentation, Juin .

[FRH 85] French R.H., (1985), "Open-Channel Hydraulics", McGraw-Hill Book Company.

[LRJ 90] Leveque R.J., Yee H.C. (1990), "A Study of Numerical Methods for Hyperbolic Conservation laws With Stiff Source Terms", Journal of Computational Physics, Vol 86 pp. 187-210.

[LRJ 92] Leveque R.J. (1992), "Numerical methods for conservation laws", Lectures in Mathematics ETH Zurich, Birkhauser Verlag.

[MLA 97] Monthe L.A, (1997), "Etude des équations aux dérivées partielles hyperboliques Application aux équations de Saint Venant", Thèse, INSA, Laboratoire de Mathématiques, LMI, UPRES-A 6085, Univ. de Rouen, France.

[RPL 81] Roe P.L ,(1981), "Approximate Riemann Solvers, Parameter vectors and difference scheme", Journal of computational Physics vol 43, pp 357-372.

[TAI 02] Taik A., (2002), "Modélisation et analyse numérique des écoulements à surface libre par un schema volumes finis et par la méthode des élément finis", thèse de Doctorat d'Etat, Juillet , EMI-Rabat, Maroc

[TMO 05] Taik A., Mouies M., Ouazar D., (July 2005),"Hydrodynamic numerical simulation of the lake of Bouregreg using finite volume method". FVCA4, Hermes Science Publishing, ISBN 1 905209 48 7, pp 691-699

[YEE 89] Yee H.C, (February 1989),"A Class of High-Resolution Explicit and Implicit Shock-Capturing Methods", NASA Technical Memorandum 101088.

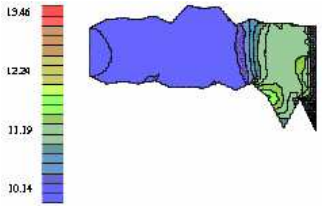

figure 7 : Iso-values distribution of depth $t = 20H31$

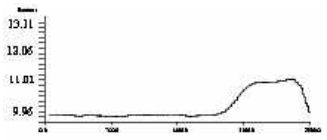

figure 7a : Depth profile $t = 20H31$, $y = -239m$

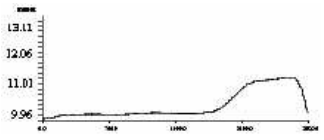

figure 7b : Depth profile $t = 20H31$, $y = 127m$

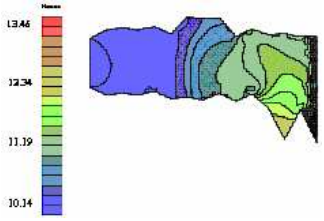

figure 8: Iso-values distribution of depth $t = 20H32$

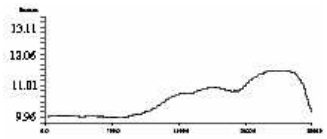

figure 8a : Depth profile $t = 20H32$, $y = -239m$

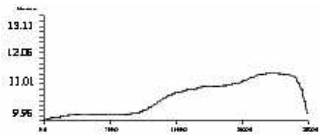

figure 8b : Depth profile $t = 20H32$, $y = 127$

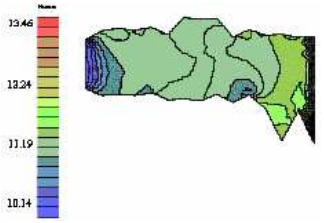

figure 9 : Iso-values distribution of depth $t = 20H34$

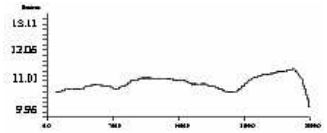

figure 9a : Depth profile $t = 20H34$, $y = -239m$

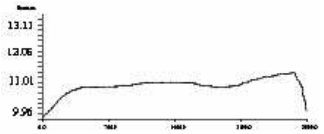

figure 9b : Depth profile $t = 20H34$, $y = 127m$

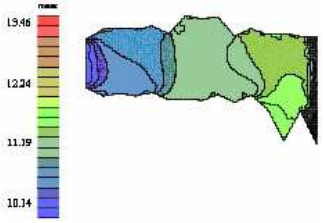

figure 10: Iso-values distribution of depth $t = 20h36$

figure 10a: Depth profile $t = 20h36$, $y = -239m$

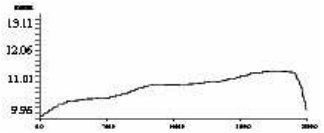

figure 10b: Depth profile $t = 20h36$, $y = 127m$

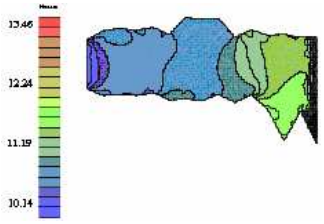

figure 11: Iso-values distribution of depth $t = 20h38$

figure 11a: Depth profile $t = 20h38$,$y = -239m$

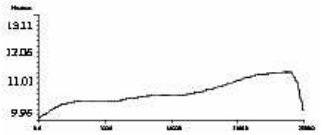

figure 11b : Depth profile $t = 20h38h$,

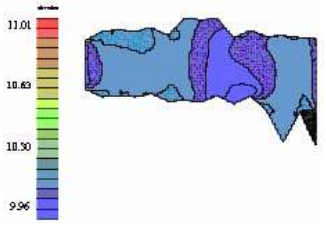

figure 12 : Iso-values distribution of depth $t = 22h$

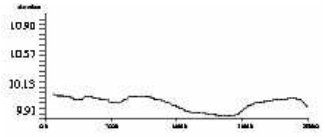

figure 12a : Depth profile $t = 22h$,$y = -239m$

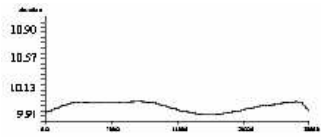

figure 12b : Depth profile $t = 22h$,$y = 127m$

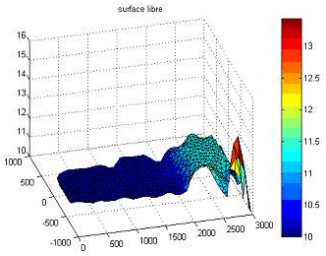

figure 13a : $3D$-Depth profile $t = 20h31$

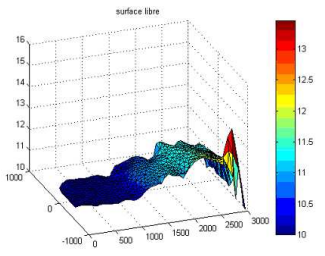

figure 13b : $3D$-Depth profile $t = 20h32$

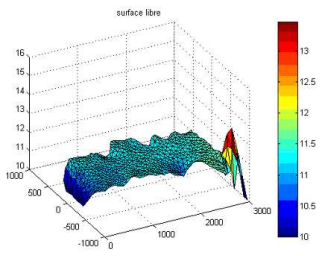

figure 13c : $3D$-Depth profile $t = 20h34$

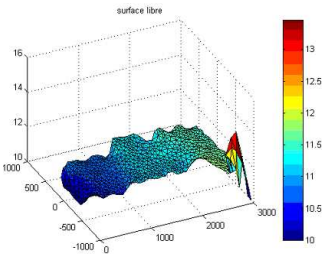

figure 13d : $3D$-Depth profile $t = 20h36$

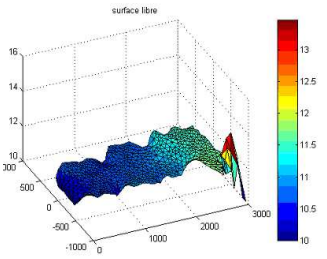

figure 13e : $3D$-Depth profile $t = 20h38$

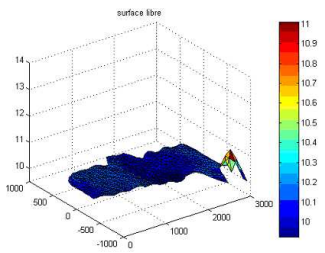

figure 13f : $3D$-Depth profile $t = 22h$

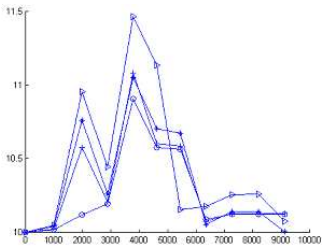

figure 14: Depth versus time (seconde) for 4 points of the channel along the line ($y \sim 13.7$), $-\triangleright$ p_1 : ($x = 2458.8m$), $-\star$ p_2: ($x = 1851m$), $-+$ p_3: ($x = 1084.7m$), $-\circ$ p_4: ($x = 772m$)